© 2016. Published by The Company of Biologists Ltd | Development (2016) 143, 276-285 doi:10.1242/dev.127506

RESEARCH ARTICLE

RING1 proteins contribute to early proximal-distal specification of the forelimb bud by restricting *Meis2* expression

Nayuta Yakushiji-Kaminatsui[1,*,‡], Takashi Kondo[1,2,3], Takaho A. Endo[4], Yoko Koseki[1,2], Kaori Kondo[1,2,3], Osamu Ohara[4], Miguel Vidal[5] and Haruhiko Koseki[1,2,‡]

ABSTRACT

Polycomb group (PcG) proteins play a pivotal role in silencing developmental genes and help to maintain various stem and precursor cells and regulate their differentiation. PcG factors also regulate dynamic and complex regional specification, particularly in mammals, but this activity is mechanistically not well understood. In this study, we focused on proximal-distal (PD) patterning of the mouse forelimb bud to elucidate how PcG factors contribute to a regional specification process that depends on developmental signals. Depletion of the RING1 proteins RING1A (RING1) and RING1B (RNF2), which are essential components of Polycomb repressive complex 1 (PRC1), led to severe defects in forelimb formation along the PD axis. We show that preferential defects in early distal specification in *Ring1A*/*B*-deficient forelimb buds accompany failures in the repression of proximal signal circuitry bound by RING1B, including *Meis1*/*2*, and the activation of distal signal circuitry in the prospective distal region. Additional deletion of *Meis2* induced partial restoration of the distal gene expression and limb formation seen in the *Ring1A*/*B*-deficient mice, suggesting a crucial role for RING1-dependent repression of *Meis2* and likely also *Meis1* for distal specification. We suggest that the RING1-MEIS1/2 axis is regulated by early PD signals and contributes to the initiation or maintenance of the distal signal circuitry.

KEY WORDS: Meis, Mouse limb development, Polycomb, Proximal-distal specification, RING1

INTRODUCTION

Polycomb group (PcG) genes were originally identified as encoding regulators of Hox genes in *Drosophila* and are evolutionarily conserved among metazoans (reviewed by Lanzuolo and Orlando, 2012; Simon and Kingston, 2009, 2013). PcG proteins form at least two multimeric complexes: Polycomb repressive complex 1 (PRC1) and PRC2. PRC1 and PRC2 cooperate to mediate transcriptional repression of target genes via histone modifications and chromatin compaction. PRC2 contains the EZH1 or EZH2 catalytic subunits that mediate histone H3 lysine 27 trimethylation (H3K27me3), while PRC1 utilizes its RING1A (RING1) and RING1B (RNF2) subunits to catalyze histone H2A monoubiquitylation at lysine 119 (H2AK119ub1). PRC1 also targets chromatin compaction by SAM domain polymerization of PHC1 and PHC2, a mammalian PH ortholog, via H3K27me3 recognition by chromodomain proteins such as CBX7 and CBX2 (Cao et al., 2002; Endoh et al., 2012; Isono et al., 2013; Kuzmichev et al., 2002). Recent studies identified a variant PRC1 complex containing RYBP (Ring1 and YY1 binding protein)/YAF (YY1-associated factor), RING1A/B and a distinct PCGF subunit (Gao et al., 2012; Tavares et al., 2012), and demonstrated that H2AK119ub1 mediated by this variant PRC1 leads to the recruitment of PRC2 and placement of H3K27me3 to initiate Polycomb repression (Blackledge et al., 2014). PcG factors are therefore expected to use diverse mechanisms for both binding and silencing of their target genes.

Studies of PcG-deficient embryonic stem cells (ESCs) showed that PcG factors contribute to the maintenance of the ESC undifferentiated state by repressing the expression of developmental genes (Boyer et al., 2006; Endoh et al., 2008; Pasini et al., 2007). Similar PcG functions have been reported in pluripotent hematopoietic stem cells, which give rise to all the blood cell lineages (Cales et al., 2008; Oguro et al., 2010). These observations support the prevailing view that PcG factors maintain epigenetic memory of gene silencing, even following cell division. On the other hand, recent studies have linked enhancer activity with the regulation of PcG-mediated gene repression. For example, a distal enhancer was shown to interfere with binding of PcG factors at the human α-globin CpG island promoter during gene activation (Lynch et al., 2012). Similarly, activation of the PcG-bound *Meis2* promoter during mouse midbrain development was accompanied by association with an active enhancer, leading to eviction of PcG factors from the promoter region (Kondo et al., 2014). These observations suggest that PcG factors are not simply a memory module for gene silencing but also play important roles in regulating gene expression by regulating promoter/enhancer interactions in response to developmental signals. However, how PcG factors contribute to morphogenetic processes, particularly during mammalian development, is poorly understood, mainly because of the complexity and dynamic nature of these events.

Limb patterning is a dynamic and complex morphogenetic process during which proliferation, regionalization and differentiation take place in a highly coordinated manner as a result of the spatiotemporally regulated expression of diverse morphogenetic signaling molecules and transcription factors (reviewed by Tabin and Wolpert, 2007; Towers and Tickle, 2009a,b; Zeller et al., 2009). Proximal-distal (PD) patterning of limb mesenchyme is coupled with limb bud outgrowth and depends on diffusible signals that define the prospective proximal and distal domains. Previous studies have suggested that the opposing activities of retinoic acid (RA) emanating from the flanking trunk mesenchyme and fibroblast growth factors (FGFs) derived from the apical ectodermal ridge (AER) contribute to

[1]Laboratory for Developmental Genetics, RIKEN Center for Integrative Medical Sciences (IMS), 1-7-22 Suehiro-cho, Tsurumi-ku, Yokohama 230-0045, Japan. [2]CREST, Japan Science and Technology Agency, 1-7-22 Suehiro-cho, Tsurumi-ku, Yokohama 230-0045, Japan. [3]KAST, Project on Health and Anti-aging, 3-25-13 Tonomachi, Kawasaki-ku, Kawasaki 210-0821, Japan. [4]Laboratory for Integrative Genomics, RIKEN IMS, 1-7-22 Suehirocho, Tsurumi-ku, Yokohama 230-0045, Japan. [5]Centro de Investigaciones Biológicas, Department of Cellular and Molecular Biology, Ramiro de Maeztu 9, Madrid 28040, Spain.
*Present address: Laboratory of Developmental Genomics, School of Life Sciences, Federal Institute of Technology, Lausanne, Lausanne 1015, Switzerland.

[‡]Authors for correspondence (nayuta.yakushiji@epfl.ch; haruhiko.koseki@riken.jp)

Received 16 June 2015; Accepted 8 December 2015

Development (2016) 143, 276-285 doi:10.1242/dev.127506

early PD limb bud specification (Cooper et al., 2011; Mariani et al., 2008; Mercader et al., 2000; Rosello-Diez et al., 2011). However, this model is still controversial, mainly because the contribution of endogenous RA has yet to be formally proven (Cunningham et al., 2011, 2013). Upon elongation of forelimb buds, interplay between the AER and underlying mesenchymal cells mediated by diffusible signals, which is interfered with by excess RA signaling, is proposed to be activated and/or stabilized to mediate development of the distal domain.

Recent studies revealed the participation of PcG factors in the PD patterning process. Limb-specific depletion of EZH2 in mice leads to skeletal defects along the PD and anterior-posterior (AP) axes (Wyngaarden et al., 2011). In zebrafish, Ring1B-mediated gene regulation has been shown to help sustain FGF signaling during pectoral fin development (van der Velden et al., 2012). However, the molecular mechanisms by which PcG factors contribute to limb patterning have remained largely unclear due to the complexity of the process and the inability to exclude potential redundancy among PcG factors.

In this study, we examined the role of PcG factors in limb patterning under conditions in which their activity is stringently limited. To achieve this, we deleted *Ring1A* (*Ring1*) and *Ring1B* (*Rnf2*), which encode members of both canonical and variant PRC1, using a *Prx1* (*Prrx1*)-*Cre* deleter mouse strain in which Cre recombinase is activated in the limb bud mesenchyme from E9.5 onward (Logan et al., 2002). Disruption of *Ring1A*/*B* resulted in severe forelimb malformation and a dysregulated gene expression pattern along the PD axis in the forelimb bud. These mutant phenotypes correlated with regionalizing signals along the PD axis, which are perturbed by excess RA signaling. Data obtained from combining chromatin immunoprecipitation (ChIP) and gene expression profiling of *Ring1A*/*B*-deficient and RA-treated forelimb buds led us to propose that the *Meis1/2* genes are concurrently regulated by RING1 proteins and PD specification signals. We further showed that additional deletion of *Meis2* substantially corrected the distal gene expression and forelimb defects seen in *Ring1A*/*B*-deficient mice. These results suggest that RING1-dependent repression of *Meis1/2* is crucial for the development of distal forelimb regions and is influenced by signals that mediate the PD specification of the forelimb bud. We thus propose that PcG factors act to mediate developmental signals at genes encoding key transcription factors to regulate the regionalization of the elongating anlagen.

RESULTS

RING1 loss affects forelimb skeletal patterning along the PD and AP axes

We first examined the expression of *Ring1A* and RING1B in developing forelimb buds. *Ring1A in situ* hybridization (ISH) analysis revealed its subtle but uniform expression at E10.5 and proximally biased expression at E12.5 (Fig. S1A). RING1B was shown by immunofluorescence (IF) analysis to be uniformly expressed at E10.5 and E12.5 (Fig. S1B). Similarly, H3K27me3 is reported to be uniformly distributed (Wyngaarden et al., 2011).

To assess the impact of PRC1 on limb formation, we examined mutant phenotypes. Previous studies have demonstrated that *Ring1A* null mice develop almost normally (del Mar Lorente et al., 2000) (Fig. S1C), whereas the *Ring1B* null is early embryonic lethal (Voncken et al., 2003). We therefore used *Ring1A* null and *Ring1B* conditional alleles and *Prx1-Cre* to deplete RING1 proteins specifically in the limb mesenchyme (Cales et al., 2008; Logan et al., 2002).

We first tested RING1B depletion efficiency by IF analysis and observed its depletion in a majority of mesenchymal cells but not in ectodermal cells, including the AER, in *Prx1-Cre;Ring1A*$^{-/-}$*;Ring1B*$^{fl/fl}$ (*Ring1A/B*-dKO) forelimb buds at E10.5 (Fig. S1D). We then investigated *Prx1-Cre;Ring1B*$^{fl/fl}$ (*Ring1B*-KO) mice because RING1B-deficient limb phenotypes have not been reported. Visual inspection of limb development at E17.5 revealed considerable shortening of the forelimbs, whereas the hindlimbs were less severely affected (Fig. 1A). Skeletal preparation showed that RING1B loss significantly affected the elongation of radius and ulna and to a lesser extent tibia and fibula (Fig. 1B, Table 1). Since this differential outcome is thought to be due to lower Cre activity in the hindlimb bud in *Prx1-Cre* deleter mice (Logan et al., 2002), we designed this study to focus on the role of RING1 proteins during forelimb development.

To test the effects of complete RING1 protein removal and *Ring1A/B* gene dosage on limb skeletal patterning, we generated *Prx1-Cre;Ring1A*$^{+/-}$*;Ring1B*$^{fl/fl}$ (*Ring1A*$^{+/-}$*;Ring1B*-KO) in addition to the *Ring1A/B*-dKO mice. Indeed, forelimb defects observed in the *Ring1B*-KO were exaggerated by additional deletion of *Ring1A* in a gene dosage-dependent manner (Fig. 1A,B, Table 1). In *Ring1A*$^{+/-}$*;Ring1B*-KO, there was a more severe shortening of the forelimbs, accompanied by various morphological alterations that were not seen in the *Ring1B*-KO, such as poor articulation of each skeletal element, decreased digit number, fusion of radius and ulna, shortening of the presumptive stylopod, and hypoplastic scapula. *Ring1A/B*-dKO fetuses possessed only rudimentary forelimbs and hindlimbs. We found only two cartilaginous elements, the origins of which could not be identified, in mesomelic forelimbs of the *Ring1A/B*-dKO. These results indicate that PRC1 plays a crucial role in limb skeletal patterning along the PD and AP axes, in agreement with an important role for PRC2 in this process (Wyngaarden et al., 2011). In the remainder of this study, we focused on how RING1 proteins contribute to PD forelimb patterning.

RING1 activity is required for distal specification of the forelimb bud

Previous studies indicated that early PD specification of forelimb buds occurs by E10.5, a conclusion based on differential expression of genes such as *Meis1/2* and *Hoxa13* between proximal and distal domains (Mariani et al., 2008; Mercader et al., 2009; Yashiro et al., 2004; Zeller et al., 2009). We investigated morphological and molecular properties of the *Ring1A/B*-dKO forelimb buds at ∼E10.5. By visual inspection, their outgrowth was indistinguishable in *Ring1A/B*-dKO and *Ring1A*$^{-/-}$ (*Ring1A*-KO) control embryos until E10.5, but then became progressively more affected at later stages. Consistent with normal forelimb bud morphology, we did not observe significant differences in the frequency of apoptotic or proliferative cells in *Ring1A/B*-dKO forelimb buds at E10.5 compared with the control (Fig. S2A).

We went on to investigate the expression of genes that demarcate proximal and distal regions of forelimb buds at E10.5 by microarray analysis (Fig. 1C). We first selected genes exhibiting at least 2-fold biased expression levels between proximal and distal domains (hereafter termed proximal and distal genes, respectively) in the control (*Ring1A*$^{-/-}$*;Ring1B*$^{fl/fl}$, designated RING1B+ in Fig. 1D) forelimb buds. We found that average expression levels of 2104 proximal and 2667 distal genes were significantly higher in proximal and distal regions, respectively (RING1B+, Fig. 1D). Next, we tested the mean expression level of these genes in the *Ring1A/B*-dKO (designated RING1B− in Fig. 1D). Interestingly, we found that these differences in gene expression levels were

Development (2016) 143, 276-285 doi:10.1242/dev.127506

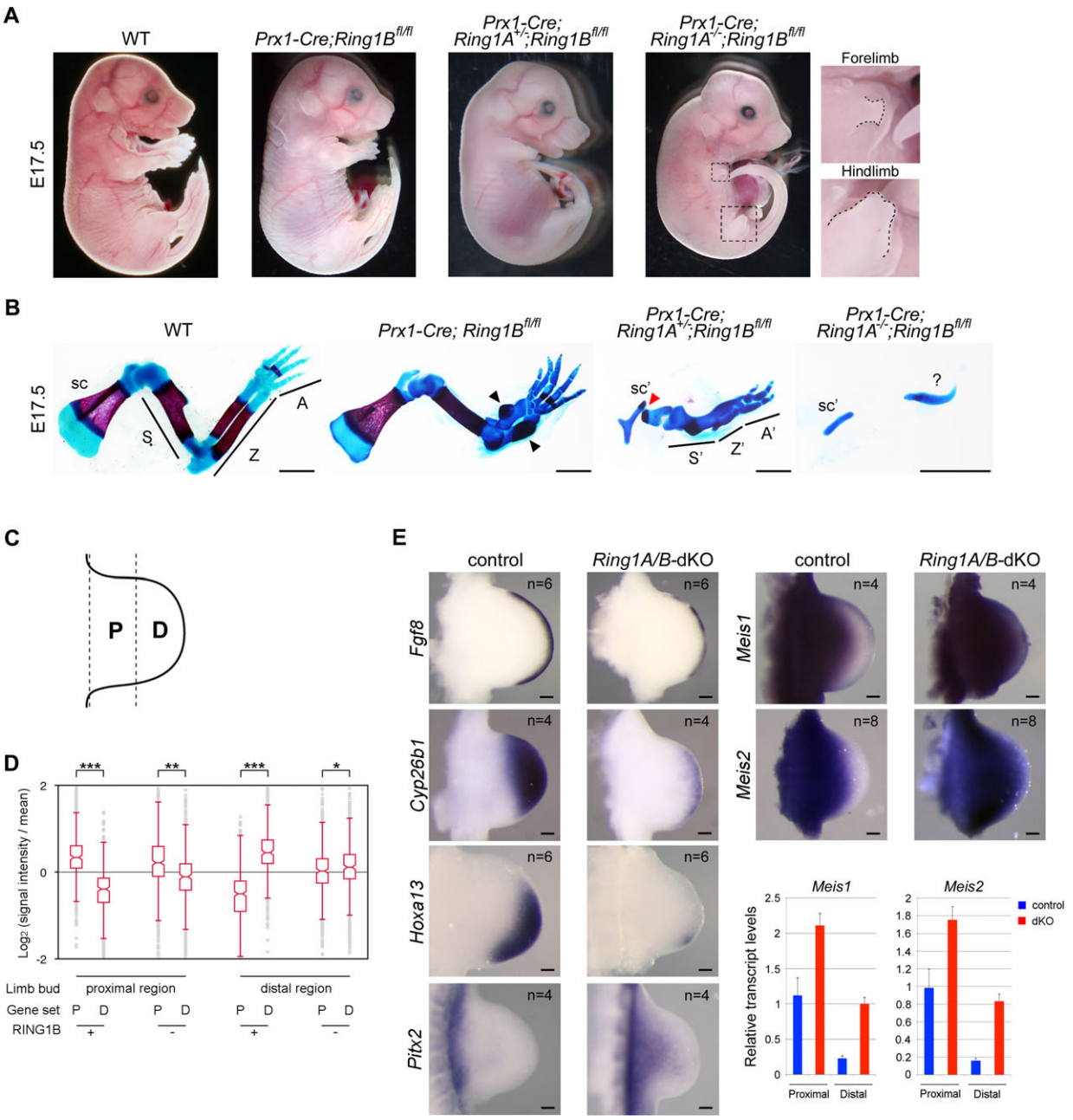

Fig. 1. RING1 contributes to PD and AP patterning of the mouse forelimb and early PD specification. (A) External appearance of each *Ring1A*/*B* mutant at E17.5, as compared with wild type (WT). Forelimb and hindlimb of the *Ring1A*/*B*-dKO are magnified to the right; dotted lines indicate the shape of the limbs. (B) Forelimb skeletal pattern of each mutant at E17.5. The zeugopod was significantly shortened in the *Prx1-Cre;Ring1B*$^{fl/fl}$ fetus (black arrowheads). The presumptive scapula was split in the *Prx1-Cre;Ring1A*$^{+/-}$*;Ring1B*$^{fl/fl}$ fetus (red arrowhead). sc, scapula; S, stylopod; Z, zeugopod; A, autopod; sc′, presumptive scapula; S′, presumptive stylopod; Z′, presumptive zeugopod; A′, presumptive autopod. The question mark indicates the unidentified cartilaginous element. (C) Control (*Ring1A*-KO, designated RING1B+ in D) and *Ring1A*/*B*-dKO (designated RING1B− in D) E10.5 forelimb buds were dissected into the proximal (P) and distal (D) portions for transcriptome analysis. (D) Expression changes resulting from RING1B depletion for proximal (gene set P) and distal (gene set D) genes. The degree of difference in expression of 2104 proximal and 2667 distal genes was most dramatically blunted in the *Ring1A*/*B*-dKO distal forelimb buds. ***$P<10^{-300}$, **$P=1.44\times10^{-83}$, *$P=1.85\times10^{-9}$, Student's *t*-test. (E) Gene expression patterns and the expression levels of *Meis1*/*2* in control (*Ring1A*-KO) and *Ring1A*/*B*-dKO forelimb buds at E10.5. Expression of *Fgf8*, *Cyp26b1*, *Hoxa13*, *Pitx2*, *Meis1* and *Meis2* was examined by ISH. Forelimb buds are oriented with proximal to the left and distal to the right. Number of specimens (*n*) is indicated in each panel. The expression level of *Meis1* and *Meis2* in forelimb buds at E10.5 was normalized to *Gapdh* and is depicted as fold change relative to the proximal region of the control. Error bars indicate the s.d. of two biological replicates. Scale bars: 1 mm in B; 100 µm in E.

significantly blunted in both proximal and distal regions of the forelimb buds (RING1B−, Fig. 1D). RING1 depletion thus induces defects in the early specification of both prospective proximal and distal domains. However, gene expression differences were more obviously blunted in the distal region ($P=1.85\times10^{-9}$) than in the proximal region ($P=1.44\times10^{-83}$). This difference suggests that gene regulation in the distal region is more dependent on RING1 activity than in the proximal region.

To further examine this tendency in genes known to be involved in limb development and/or limb morphogenesis, we

Development (2016) 143, 276-285 doi:10.1242/dev.127506

Table 1. Summary of forelimb skeletal deformities observed in *Ring1A/B* mutant and/or excess RA-treated mice

Genotypes	RA treatment	Scapula	Stylopod	Zeugopod	Digit number	Severity	*n* (%)
Ring1B$^{fl/+}$ or *Ring1B*$^{fl/fl}$	–	–	–	–	–	0	10/10 (100)
	+	–	–	–	–	0	3/15 (20)
		–	–	+	–	1	6/15 (40)
		–	+	+	+	3	6/15 (40)
Prx1-Cre;Ring1B$^{fl/+}$	–	–	–	–	–	0	10/10 (100)
	+	–	–	–	–	0	3/8 (37.5)
		–	+	+	+	3	5/8 (62.5)
Prx1-Cre;Ring1B$^{fl/fl}$	–	–	–	+	–	1	10/10 (100)
	+	+	+	+	+	4	6/6 (100)
Prx1-Cre;Ring1A$^{+/-}$*;Ring1B*$^{fl/fl}$	–	+	+	+	+	4	5/5 (100)
Prx1-Cre;Ring1A$^{-/-}$*;Ring1B*$^{fl/fl}$	–	+	+	+	+	5	8/8 (100)
Cyp26b1$^{-/-}$	–	–	+	+	+	3	2/2 (100)
Prx1-Cre;Cyp26b1$^{-/-}$*;Ring1B*$^{fl/fl}$	–	+	+	+	+	4	3/3 (100)
Prx1-Cre;Ring1A$^{-/-}$*;Ring1B*$^{fl/fl}$*;Meis2*$^{fl/fl}$	–	+	+	+	+	5*	6/6 (100%)

The presence of morphological abnormalities in scapula, stylopod and zeugopod and changes in digit number are indicated by +, and their absence by –. After observation of skeletal preparations, we scored the severity of the forelimb phenotypes from 0 to 5, according to the number of + scores, except for the *Prx1-Cre;Ring1A*$^{-/-}$*;Ring1B*$^{fl/fl}$ and *Prx1-Cre;Ring1A*$^{-/-}$*;Ring1B*$^{fl/fl}$*;Meis2*$^{fl/fl}$ mice. Because of extensive alterations in *Prx1-Cre;Ring1A*$^{-/-}$*;Ring1B*$^{fl/fl}$ mice, we could not accurately determine the origin of each skeletal element and thus scored the phenotypes as 5. Furthermore, this phenotype was partially restored in *Prx1-Cre;Ring1A*$^{-/-}$*;Ring1B*$^{fl/fl}$*;Meis2*$^{fl/fl}$ mice and we thus scored it as 5*.

selected 112 genes based on Gene Ontology (GO) and analyzed their expression (Fig. S2B). These limb-related genes included 31 distal and 13 proximal genes (Fig. S2B). As revealed by clustering analysis, limb-related distal genes tended to be downregulated, whereas proximal genes were upregulated in the distal region of *Ring1A/B*-dKO forelimb buds (Fig. S2C). Consistent with this trend, the gene expression profile in the distal region of the *Ring1A/B*-dKO was more closely related to the proximal region than the distal region of the control based on the correlation coefficient (Fig. S2C,D). These results suggest that acquisition of distal identity in the forelimb bud is more dependent than proximal identity on RING1 activity.

We validated these results by ISH analysis (Fig. 1E, Fig. S2E), first testing *Fgf8*, *Cyp26b1*, *Shh* and *Grem1*, which exhibit distally restricted expression and are known to contribute to distal development. Consistent with the microarray data, we found that the expression of these genes was considerably reduced in *Ring1A/B*-dKO forelimb buds. By contrast, expression of *Pitx2* was distally expanded (Fig. 1E). Expression of *Rarb* (Niederreither et al., 2002) also showed a major difference, although not by ISH but by RT-qPCR analysis of the distal forelimb bud (Fig. S2E). We also observed a considerable downregulation of *Hoxa13* but only a slight change in *Hoxa11* in the *Ring1A/B*-dKO (Fig. 1E, Fig. S2E), even though Hox genes are known as the classical PcG targets. We further examined *Meis1/2*, which are known proximal marker genes (Mercader et al., 1999, 2000) but are not categorized as limb-related genes by GO, and found that their expression was distally expanded in the *Ring1A/B*-dKO forelimb buds (Fig. 1E). RT-qPCR analysis confirmed activation of *Meis1/2* expression in the distal region of these embryos, reaching levels observed in the control proximal region (Fig. 1E). We therefore suggest a role of RING1 proteins in establishing a coordinated gene expression pattern that demarcates the distal region of the forelimb bud by E10.5. Importantly, *Fgf8* expression in the AER was considerably downregulated irrespective of mesenchyme-specific deletion of *Ring1B* (Fig. S1D). Together with downregulation of *Cyp26b1*, *Shh* and *Grem1* in the *Ring1A/B*-dKO, RING1 proteins in the mesenchyme are suggested to contribute to establishing or maintaining signaling circuitry that mediates interactions between the AER and underlying mesenchyme and the subsequent specification of the prospective distal domain of forelimb buds.

RING1 activity is correlated with regionalizing signals of forelimb buds

To explore how RING1 activity contributes to early distal specification of forelimb buds, we next addressed whether its activity is linked to early PD specification signals. Since signaling circuitry involving the AER and underlying mesenchyme has been reported to be inhibited by high levels of RA, which is thought to mimic an exaggerated version of proximal signals (Probst et al., 2011), we investigated whether RING1 activity could be influenced by excess RA signaling. We thus examined whether transient increases in RA signaling at E10.5 could modify the limb defects in *Ring1B* mutant mice.

All-trans RA (50 mg/kg body weight) was orally administered once to pregnant *Ring1B*$^{fl/fl}$ females that had been mated with *Prx1-Cre;Ring1B*$^{fl/+}$ males. A single administration of RA at E10.5 variably affected *Ring1B*$^{fl/+}$ or *Ring1B*$^{fl/fl}$ fetuses at E17.5, ranging from no major changes (3/15) or subtle shortening of the zeugopod (6/15) to moderate shortening of both zeugopod and stylopod and a decreased number of digits (6/15) (Fig. 2A left, Table 1). *Prx1-Cre;Ring1B*$^{fl/+}$ fetuses at E17.5 were also variably affected by RA administration, but tended to exhibit more exaggerated forelimb deformities (5/8) than *Ring1B*$^{fl/+}$ or *Ring1B*$^{fl/fl}$ fetuses (Fig. 2A middle, Table 1). By contrast, *Ring1B*-KO fetuses at E17.5 were uniformly affected by RA administration and this exaggerated limb phenotype was similar to that of *Ring1A*$^{+/-}$*;Ring1B*-KO fetuses in regards to the severity (6/6) (Fig. 2A right, compared with Fig. 1B).

We confirmed this synergy using a *Cyp26b1* mutant, in which early distal specification is impaired, probably owing to increased endogenous RA activity (Yashiro et al., 2004). We investigated skeletal phenotypes of *Cyp26b1;Ring1B*-dKO mice and found that the phenotype was more severe than in the respective single-knockout mice (Fig. 2B). Together, these results show that residual RING1 activity in *Ring1B*-KO is dampened by excess RA signals. These observations suggest that RING1 activity could be correlated with signals that mediate PD patterning of the forelimb. Since excess RA did not considerably alter RING1B expression in either the proximal or distal region (Fig. S3A), it might affect the gene regulatory activity of RING1 at target genes. We thus presume that RING1 target genes that are regulated by early PD specification signals may play a role in early distal specification.

Development (2016) 143, 276-285 doi:10.1242/dev.127506

Regulation of *Meis1/2* by RING1 and PD specification signals

We next aimed to identify a group of genes concurrently regulated by RING1 and early PD signals. Such genes should be bound and repressed by RING1B but be induced by excess RA in the distal region of the forelimb bud. We used ChIP assays combined with microarray technology (ChIP-on-chip analysis) to identify genes bound by RING1B and marked by H3K27me3 in E10.5 forelimb buds. We identified 2085 genes bound by RING1B, and these are a subset of 5010 H3K27me3-positive genes (Fig. S3B, Table S1). RING1B targets in forelimb buds significantly overlapped with those in ESCs (Endoh et al., 2008). RING1B-bound genes were significantly derepressed in the distal region of forelimb buds in *Ring1A/B*-dKO at E10.5 (Fig. 3A,B).

We next identified genes activated by excess RA in distal forelimb buds. We treated wild-type embryos at E10.25 with a single oral administration of all-trans RA (100 mg/kg) to pregnant females and performed transcriptome analysis on the distal region of the forelimb buds at E10.5. We found that proximal genes were significantly upregulated by excess RA (Fig. 3A,B). We identified 70 genes that are bound by RING1B, activated by RING1 loss or excess RA, and are normally repressed in the distal region, 27 of which encode transcription factors (Fig. 3C).

To investigate whether RING1B preferentially binds to these 27 genes in the distal region of the forelimb buds, we performed ChIP-seq analysis using E11.5 proximal and distal regions. In the distal region, we found the most biased RING1B binding around transcription start sites (TSSs) of the *Meis1* gene, with *Meis2* as a second hit (Fig. S3C,D). At both *Meis1* and *Meis2*, we observed intense RING1B binding around the TSS and the 3′ region, which we designated as a RING1B binding site (RBS) in our previous study (Kondo et al., 2014), and more RING1B accumulation in the distal than in the proximal region (Fig. 3D, Fig. S3E). We further confirmed skewed RING1B binding in the distal domain at the TSS and RBS by ChIP-qPCR analysis (Fig. 3E, Fig. S3F). Consistent with the RING1B binding, we observed enrichment of H3K27me3 at both TSS and RBS of *Meis1/2* (Fig. 3E, Fig. S3F) and close TSS/RBS contact at *Meis2* in the distal region (Fig. 3G). We then investigated whether H3K27me3 accumulation at the TSS region and the TSS/RBS association at *Meis2* depend on RING1 activity and found significant reduction of H3K27me3 and dissociation of TSS and RBS in the distal region of *Ring1A/B*-dKO forelimb buds (Fig. 3F-H). By contrast, no obvious change was seen for H3K4me3 accumulation at these genomic regions in the distal region of the *Ring1A/B*-dKO (Fig. 3F).

Together with the expression of *Meis1* and *Meis2* in the distal region of *Ring1A/B*-dKO forelimb buds at E10.5 (Fig. 1E), these observations indicate that RING1 proteins directly contribute to the repression of both genes in the distal region of the forelimb bud. Notably, both *Meis1* and *Meis2* were shown to be activated by excess RA in the distal region of forelimb buds (Mercader et al., 2000; Yashiro et al., 2004) (N.Y.-K., unpublished data), and overexpression of *Meis1* or *Meis2* has been reported to impair the expression of distal genes and distal limb development (Capdevila et al., 1999; Mercader et al., 1999, 2009). We therefore hypothesized that RING1-mediated repression of *Meis1* and/or *Meis2* could be an important step in the early specification of the distal region of the forelimb bud.

RING1-dependent repression of *Meis2* is involved in early distal specification of forelimb buds

To test the above hypothesis, we examined whether additional mutation of *Meis2* could restore the forelimb defects resulting from RING1 deficiency. Since a constitutive mutant allele of *Meis2* exhibits haploinsufficiency and the mice do not survive the perinatal period (T.K., unpublished data), we generated a conditional allele (*Meis2*^{fl}) (Fig. S4). We first examined the forelimb skeletal phenotypes of *Prx1-Cre;Meis2*$^{fl/fl}$ (*Meis2*-KO) fetuses at E17.5 and found no major changes, as reported for *Meis1*-deficient mice (Fig. 4A) (Azcoitia et al., 2005; Hisa et al., 2004).

We then generated *Prx1-Cre;Ring1A*$^{-/-}$*;Ring1B*$^{fl/fl}$*;Meis2*$^{fl/fl}$ (*Ring1A/B;Meis2*-tKO) mice and observed considerable

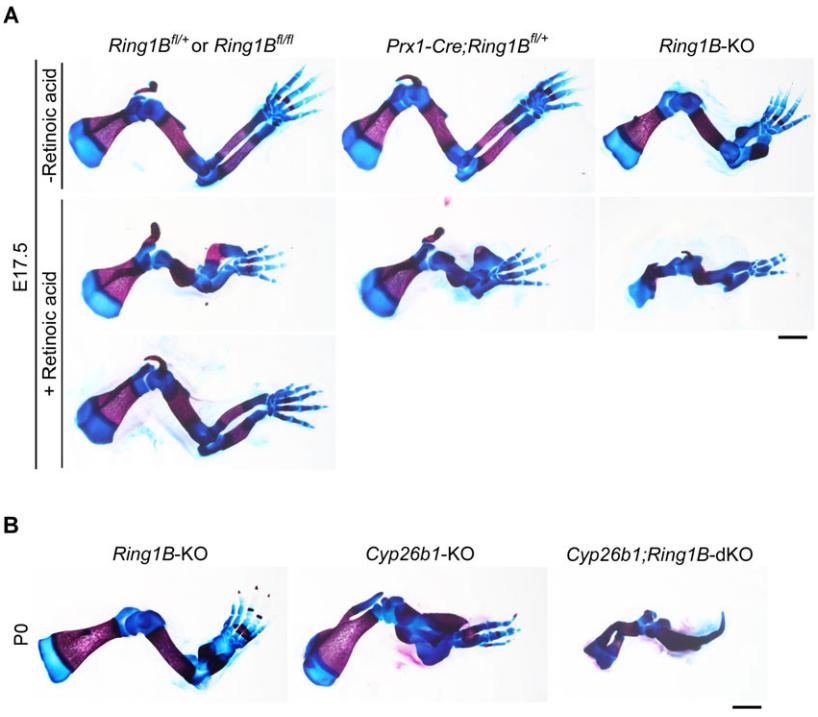

Fig. 2. Synergistic forelimb defects caused by *Ring1B* deficiency and excess RA signaling. (A) Exaggerated forelimb skeletal defects in *Ring1B* mutants caused by all-trans RA. Pharmacological effects of all-trans RA on the control (*Ring1B*$^{fl/+}$ or *Ring1B*$^{fl/fl}$, left), *Prx1-Cre;Ring1B*$^{fl/+}$ (middle) and *Ring1B*-KO (*Prx1-Cre;Ring1B*$^{fl/fl}$, right) fetuses at E17.5 are shown. (B) Genetic interactions between *Ring1B* and *Cyp26b1* mutations during forelimb patterning. Forelimb skeletal patterns of *Ring1B*-KO, *Cyp26b1*$^{-/-}$ (*Cyp26b1*-KO) and *Prx1-Cre;Ring1B*$^{fl/fl}$*;Cyp26b1*$^{-/-}$ (*Ring1B;Cyp26b1*-dKO) in P0 newborn mice are shown. Scale bars: 1 mm.

Development (2016) 143, 276-285 doi:10.1242/dev.127506

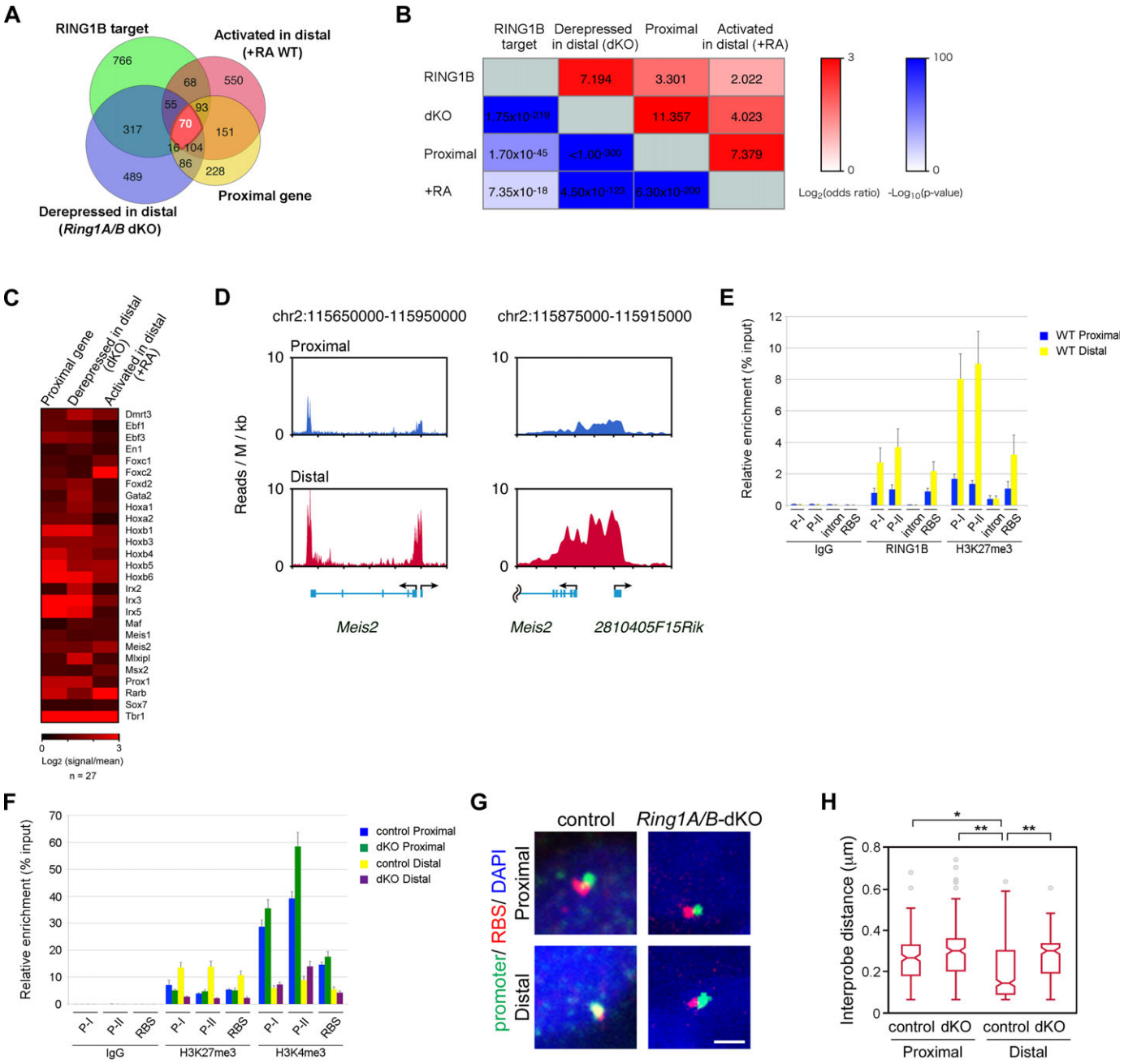

Fig. 3. RING1 activity and PD specification signals converge at Meis genes. (A) Venn diagram representation for the overlap among proximal genes that are normally repressed by RING1B but can be activated by RA signals in the distal region of the forelimb bud. We investigated genes that are bound by RING1B in the distal region (RING1B target), derepressed in the distal region of *Ring1A*/*B*-dKO, activated by excess RA (+RA WT) and preferentially expressed in the proximal region (proximal gene) at E10.5 and tested their overlap. The number of genes in each category is indicated. (B) A numerical representation for the correlations between respective gene groups. Odds ratios for overlaps of respective gene groups are shown in the red panels and *P*-values are shown in the blue panels. (C) Heat map representation for expression changes of 27 transcription factor genes included among 70 proximal genes that are bound by RING1B, derepressed in *Ring1A*/*B*-dKO and activated by excess RA signals. The left column shows expression differences between proximal and distal regions in the control (*Ring1A*-KO) forelimb buds. The middle column shows the expression changes in the distal region of *Ring1A*/*B*-dKO. The right column shows the expression changes caused by excess RA in the distal region of wild-type forelimb buds. (D) RING1B binding at the *Meis2* locus in E11.5 proximal and distal forelimb buds revealed by ChIP-seq analysis. Right-hand panels show the binding around the TSS. Note the intense RING1B enrichment around the TSS and RBS (RING1B binding site at the 3′ region of *Meis2*). (E) Intense accumulation of RING1B and H3K27me3 around the TSS and RBS of the *Meis2* locus in the distal region of forelimb buds at E10.5 as revealed by ChIP-qPCR analysis. Binding of RING1B and H3K27me3 at sites P-I and P-II, which are both located around the TSS, intronic region and RBS were compared between proximal and distal regions of E10.5 forelimb buds. Error bars indicate s.e.m. of three biological replicates. (F) RING1-dependent accumulation of H3K27me3 around the TSS and RBS of the *Meis2* locus in the distal region of forelimb buds at E10.5 as revealed by ChIP-qPCR analysis. Presence of H3K27me3 and H3K4me3 at P-I, P-II and RBS were compared between the control (*Ring1A*-KO) and *Ring1A*/*B*-dKO in proximal and distal regions of E10.5 forelimb buds. Error bars indicate the s.e.m. of three biological replicates. (G) RING1-dependent promoter/RBS association at *Meis2* in the distal region of E10.5 forelimb buds as revealed by DNA-FISH analysis. The subnuclear localization of promoter (green) and RBS (red) regions was examined in the proximal and distal regions of control (*Ring1A*-KO) and *Ring1A*/*B*-dKO forelimb bud at E10.5. Scale bar: 1 μm. (H) Box plot representation for the DNA-FISH analysis. The box plots show the interprobe distances (μm) in each tissue. Over 200 loci were observed in this experiment. $^{**}P<10^{-300}$, $^{*}P=2.1\times10^{-15}$, Student's *t*-test.

Development (2016) 143, 276-285 doi:10.1242/dev.127506

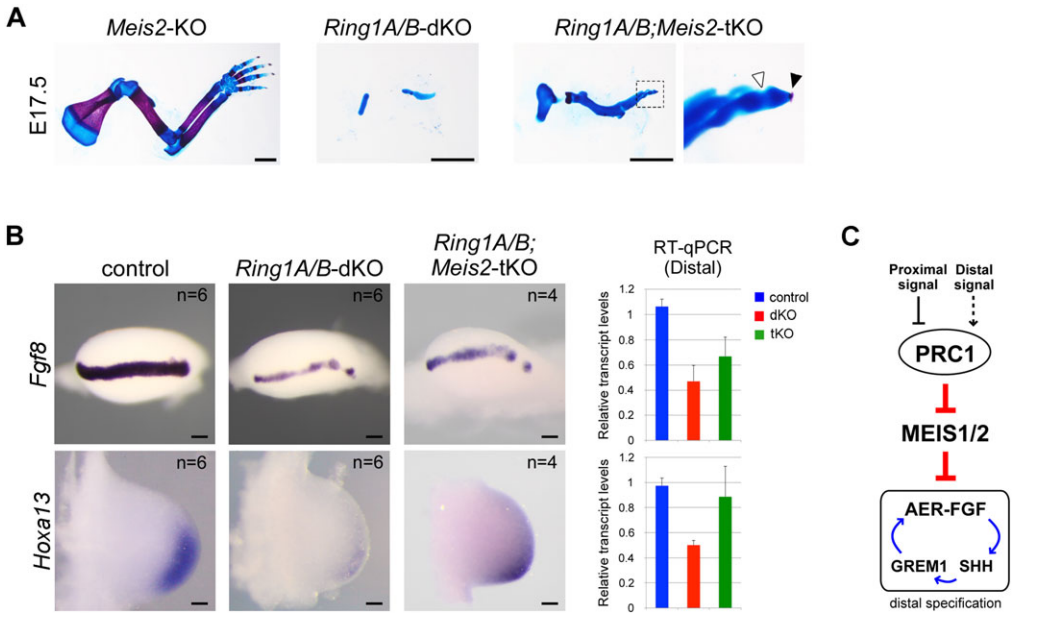

Fig. 4. RING1-mediated repression of *Meis2* is a key process for distal specification. (A) Partial restoration of forelimb skeletal defects in *Ring1A*/*B*-dKO by *Meis2* mutation. Forelimb skeletal patterns of *Meis2*-KO, *Ring1A*/*B*-dKO and *Ring1A*/*B;Meis2*-tKO are shown. The boxed region is enlarged to the right. White and black arrowheads indicate segmentation of the distal region and ossification of phalangeal bones, respectively, which were not seen in *Ring1A*/*B*-dKO. (B) Partial restoration of *Fgf8* and *Hoxa13* expression in forelimb buds of *Ring1A*/*B*-dKO by *Meis2* mutation. (Left) Expression of *Fgf8* and *Hoxa13* in the control (*Ring1A*-KO), *Ring1A*/*B*-dKO and *Ring1A*/*B;Meis2*-tKO forelimb buds at E10.5 was examined by ISH analysis. Numbers of specimens are shown in each panel. (Right) The expression level of *Fgf8* and *Hoxa13* in the distal region of forelimb buds was examined by RT-qPCR. Results were normalized to *Gapdh* and are shown as fold change relative to the distal region of the control. Error bars indicate s.d. of two biological replicates. (C) A schematic representation of the role of the RING1-MEIS1/2 axis in elongating forelimb buds. MEIS1/2 contribute to suppress distal specification via repressing the SHH-GREM1-AER-FGF loop. RING1-dependent repression of Meis genes is an important process for proper distal specification and/or maintenance of the SHH-GREM1-AER-FGF loop in the prospective distal region. The RING1 function is probably repressed or activated by a proximal or distal signal, respectively. Scale bars: 1 mm in A; 100 µm in B.

elongation of the forelimb skeleton and obvious segmentation and ossification of distal components (6/6, Fig. 4A, Table 1). We thus concluded that the limb defects observed in the *Ring1A/B*-dKO were partially rescued by a *Meis2* mutation. We further examined whether the downregulation of distal gene expression in *Ring1A/B*-dKO limb buds was restored by the *Meis2* mutation and observed that the expression pattern and level of *Fgf8* and *Hoxa13* were partially, but substantially, restored in the *Ring1A/B;Meis2*-tKO (Fig. 4B). Partial rescue of the *Ring1A/B*-dKO phenotype by the additional *Meis2* mutation implies that RING1-dependent repression of *Meis2* is crucial for distal specification, but that *Meis2* is not an exclusive RING1 target gene.

Taken together, these results suggest that RING1 activity and PD specification signals converge on a set of essential regulators of PD patterning, such as *Meis2* and likely also *Meis1*, to facilitate distal forelimb bud development.

DISCUSSION

In this study, we reveal a role for RING1 proteins in regulating the early PD regionalization of forelimb buds that occurs at ∼E10.5. RING1 activity preferentially contributes to distal forelimb development by repressing the expression of proximal genes, including *Meis1/2*, in the prospective distal domain of the outgrowing forelimb bud. Partial phenotypic correction of *Ring1A/B*-deficiency by additional deletion of *Meis2* suggests that RING1-dependent repression of *Meis2*, and likely also *Meis1*, is an important process for proper distal specification (Fig. 4C).

This study further suggests that the RING1-MEIS1/2 axis is functionally correlated with signaling pathways that contribute to PD specification. During distal specification, antagonistic features of early proximal and distal signals emanating from trunk mesenchyme and AER, respectively, are reported to help establish the SHH-GREM1-AER-FGF loop in the prospective distal region of elongating forelimb buds that subsequently facilitates distal development (Probst et al., 2011). Our study shows that RING1-dependent *Meis1/2* repression is involved in the initiation and/or maintenance of the distal specification signal loop. On the other hand, excess RA signaling, which mimics an exaggerated version of proximal signals, has been reported to disturb distal specification loop formation concomitant with *Meis1/2* repression in the prospective distal domain. Together with synergistic impairments of distal forelimb development by excess RA and *Ring1B* mutation (Fig. 2), RING1-dependent repression of *Meis1/2* is thought to be regulated by early PD signals. In summary, we propose that the RING1-MEIS1/2 axis helps to initiate and/or stabilize the distal signal circuitry by sensing the polarization of early PD signals, which is likely to occur upon progressive separation of proximal and distal domains due to forelimb outgrowth, and then to demarcate the prospective distal domain (Fig. 4C).

The molecular nature of the early proximal signals is still controversial, but RA is a plausible candidate for an early proximal signal (Probst et al., 2011; Yashiro et al., 2004). RING1-dependent activation of *Cyp26b1* (Fig. 1E), which contributes to distal forelimb development, possibly by degrading RA, might support this model. However, defects of hindlimb elongation in *Ring1A/B*-dKO (Fig. 1A) could suggest that RA is not necessarily an exclusive signaling molecule to regulate the RING1-MEIS1/2 axis (Cunningham et al., 2011, 2013). Consistent with this model, we observed slight but considerable reduction of *Fgf8* expression at the AER of *Ring1A/B*-dKO forelimb buds as early as E9.5 (N.Y.-K.,

Development (2016) 143, 276-285 doi:10.1242/dev.127506

unpublished data). Importantly, this finding further suggests the involvement of other classes of RING1 targets that are likely to act at an earlier stage than *Meis2* repression. These possibilities require experimental elucidation in the future.

Our observations imply that robust and stable repression of target genes is not the sole activity of PcG factors; they also mediate inducible repression under the regulation of morphogenetic signals. Notably, PcG factors have been reported to be linked with RA, FGFs, SHH and MAP kinase pathways (Schwermann et al., 2009; Shi et al., 2014; van der Velden et al., 2012; Wu et al., 2013; Yokobayashi et al., 2013). By such interactions with signaling pathways, PcG factors may contribute to the compartmentalization of outgrowing or enlarging fetal tissues by regulating the expression of developmental genes. In addition, the skeletal phenotypes of the *Ring1A/B*-dKO forelimb may not simply be due to the dysregulation of PD patterning but might also involve defects in AP patterning, skeletogenesis and/or chondrogenesis as reported previously (Schwarz et al., 2014; van der Velden et al., 2013; Wyngaarden et al., 2011). RING1 proteins could help to coordinate and integrate various morphogenetic signals to accomplish forelimb patterning. However, the underlying mechanisms by which PcG factors are linked to signaling pathways remain to be elucidated. Identification in this study of *Meis1/2* as common targets of RING1 and PD specification signals provides a good entry point for further study to elucidate the molecular mechanisms underlying the signal-dependent regulation of PcG activity.

This and previous studies suggest a role for PcG factors during induced repression and activation of Meis genes in the forelimb bud and midbrain, respectively (Kondo et al., 2014). RING1-associated PcG factors thus play a role in both the stable repression and inducible expression of their target genes. Consistent with the functional diversity of PcG factors during development, recent biochemical studies suggest that RING1 proteins are components of several different PRC1-related complexes that can be discriminated by their biochemical properties, as represented by PCGF factors that interact with RING1B (Blackledge et al., 2014; Gao et al., 2012). We thus suspect that the use of different PRC1-related complexes could at least partly account for the functional diversity of PcG factors during development. Indeed, our preliminary analysis of *Pcgf3* knockout fetuses revealed zeugopod shortening similar to that of the *Ring1B*-KO, whereas *Pcgf2* (*Mel18*) or *Pcgf4* (*Bmi1*) mutants, or even their compound mutants, did not have any zeugopod defects (N.Y.-K. and H.K., unpublished data) (Akasaka et al., 2001). We thus suggest that different PRC1-related complexes play different roles at each phase of the developmental regulation of *Meis1/2* expression. This model and its applicability to other target genes are under investigation.

MATERIALS AND METHODS

Animals

Prx1-Cre, *Ring1A*$^{-/-}$, *Ring1B*$^{fl/fl}$ and *Cyp26b1*$^{+/-}$ mouse lines were described previously (Cales et al., 2008; del Mar Lorente et al., 2000; Logan et al., 2002; Yashiro et al., 2004). Conditional deletion of *Ring1B* was achieved by crossing *Prx1-Cre;Ring1B*$^{fl/+}$ males with *Ring1B*$^{fl/fl}$ females. For the production of *Ring1A/B*-dKO embryos, *Prx1-Cre;Ring1A*$^{-/-}$;*Ring1B*$^{fl/+}$ males were mated with *Ring1A*$^{-/-}$;*Ring1B*$^{fl/fl}$ females and *Ring1A*$^{-/-}$;*Ring1B*$^{fl/fl}$ or *Ring1A*$^{-/-}$;*Ring1B*$^{fl/+}$ embryos were used as controls. The *Meis2*$^{fl/fl}$ mouse is described in Fig. S4. All animal experiments were carried out according to institutional guidelines for the care and use of laboratory animals of the RIKEN, Yokohama Institute, Japan.

Skeletal preparation and whole-mount *in situ* hybridization (ISH)

Skeletons of fetal and newborn mice were stained with Alizarin Red and Alcian Blue as described previously (Parr and McMahon, 1995). Whole-mount ISH was performed according to Wilkinson and Nieto (1993). The number of biological replicates is shown in figures.

Immunostaining and apoptosis detection

E10.5 embryos were subject to immunostaining and apoptosis detection using the ApopTag In Situ Detection Kit (Chemicon) as described in the supplementary Materials and Methods.

Retinoic acid (RA) treatment and sampling

RA treatment was performed as previously described (Yashiro et al., 2004). Fetuses obtained by crossing *Ring1B*$^{fl/fl}$ females with *Prx1-Cre;Ring1B*$^{fl/+}$ males received all-trans RA at a dose of 50 mg/kg body weight at E10.5 by maternal oral administration, and they were sampled at E17.5. Control pregnant females were administered only sesame oil.

Chromatin immunoprecipitation (ChIP) analysis

Forelimb buds at E10.5 and E11.5 from wild-type embryos, *Ring1A*$^{-/-}$ or *Prx1-Cre;Ring1A*$^{-/-}$;*Ring1B*$^{fl/fl}$ were used for ChIP-on-chip, ChIP-seq and ChIP-qPCR. Forelimb buds were fixed in 1% formaldehyde in PBS for 20 min at room temperature, washed three times with cold PBS containing protease inhibitors and stored at −80°C before use. ChIP was performed as described previously (Endoh et al., 2012). For each immunoprecipitation, 100 µl anti-RING1B (Atsuta et al., 2001), 4 µg anti-RING1B (39663, Active Motif), 3 µg anti-H3K27me3 (07-449, Millipore) and 3 µg anti-H3K4me3 (07-473, Millipore) were used.

ChIP-on-chip and ChIP-seq

Purified immunoprecipitated and whole-cell extract (input) DNAs were amplified using the double-round T7 RNA polymerase-based amplification method (van Bakel et al., 2008). Labeled DNA samples were hybridized to the Mouse Promoter ChIP-on-chip 244 K Microarray (G4495A#14716, 14717, Agilent Technologies), washed and scanned according to the mammalian ChIP-on-chip protocol (Agilent Technologies). ChIP-seq was performed as described previously (Kondo et al., 2014).

Microarray

Forelimb buds at E10.5 from each embryo were dissected into proximal and distal portions. Total RNA was extracted using the RNeasy Micro Kit (Qiagen) following the manufacturer's protocol. cDNA was synthesized using the GeneChIP 3′ IVT Express Kit (Affymetrix) or Ovation RNA Amplification System V2 (Nugen) according to the manufacturers' protocols. Labeled samples were hybridized to Affymetrix GeneChip Mouse Genome 430 2.0 arrays (Affymetrix) to assess and compare the overall gene expression profiles.

Data analysis

Fold enrichment of ChIP-chip signals between input and immunoprecipitated DNA was calculated using an in-house program on probes that had a significantly different signal level from background ($P<10^{-7}$). Whole intensities were normalized using rank consistency filtering and binding regions were determined as previously reported (Endoh et al., 2012). Sequences retrieved in ChIP-seq experiments were aligned on the mouse genome (mm9) using the Bowtie 2 program (Johns Hopkins University) and accumulated reads were normalized using total mapped reads and counted using our in-house program. Genes were represented by the mapped normalized counts around the TSS (−4 kb to +4 kb).

Microarray signals were converted into numeric values with statistical calls using the MAS5.0 algorithm provided as R packages. When multiple probes were assigned to a single gene, expression changes between two samples were indicated as the geometric mean of all probes for a gene.

GO analysis was performed using the annotation database in Gene Ontology (http://geneontology.org/). Enrichment of genes having a specific GO term was counted and statistically evaluated using a hypergeometric distribution.

Development (2016) 143, 276-285 doi:10.1242/dev.127506

Reverse transcription

RNA extraction and cDNA synthesis were performed using the RNeasy Micro Kit (Qiagen) and SuperScript VILO (Invitrogen), respectively, according to the manufacturers' protocols.

Quantitative real-time PCR (RT-qPCR)

RT-qPCR was performed on an Mx3005P system (Agilent Technologies) using the Brilliant SYBR Green QPCR Master Mix (Agilent Technologies). RT-qPCR and ChIP-qPCR were carried out with two and three biological replicates, respectively. Primer sequences are listed in Table S2.

DNA-fluorescent *in situ* hybridization (FISH) analysis

FISH analyses on sections were carried out according to a protocol described previously (Kondo et al., 2014). Mouse embryos were fixed with 4% paraformaldehyde (PFA), embedded in paraffin and sectioned at 5 µm thickness. After deparaffinization, sections were soaked in HistoVT One solution (Nakalai Tesque, 06380-05) in glass vessel, and the glass vessel containing sections was placed in boiling water for 20 min. Immediately following this treatment, sections were washed with distilled water to remove detergents and used for FISH.

Accession numbers

Microarray and ChIP-on-chip data are available from the NCBI Gene Expression Omnibus repository under accession number GSE70077. The ChIP-on-chip data for H3K27me3 and RING1B in ESCs and ChIP-seq data for RING1B are from GSE38650 (ESCs, H3K27me3, RING1B) and GSE48464 (limb buds, RING1B).

Acknowledgements

We thank Dr Hiroshi Hamada (Osaka University, Japan) for providing *Cyp26b1*$^{+/-}$ mice and *Cyp26b1* and *Pitx2* plasmids. We also thank our animal facility group staff for animal care and 2-cell transplantations to foster mothers. N.Y.-K. also thanks Dr Denis Duboule and members of the Duboule laboratory for their generous support.

Competing interests

The authors declare no competing or financial interests.

Author contributions

N.Y.-K. and H.K. designed the experiments; N.Y.-K. and T.K. performed the experiments; T.A.E. and O.O. performed sequencing and data analyses; Y.K., K.K. and M.V. generated compound mutants; N.Y.-K., T.A.E. and H.K. wrote the manuscript.

Funding

This work was supported by Grants-in-Aid for Scientific Research from the Ministry of Education, Culture, Sports, Science and Technology of Japan (to H.K.), CREST (to H.K. and T.K.), Special Postdoctoral Researcher Program of RIKEN (to N.Y.-K.), Regional Innovation Program from MEXT (to T.K.) and SIP from Cabinet Office (to T.K. and H.K.).

Supplementary information

Supplementary information available online at
http://dev.biologists.org/lookup/suppl/doi:10.1242/dev.127506/-/DC1

References

Akasaka, T., van Lohuizen, M., van der Lugt, N., Mizutani-Koseki, Y., Kanno, M., Taniguchi, M., Vidal, M., Alkema, M., Berns, A. and Koseki, H. (2001). Mice doubly deficient for the Polycomb group genes Mel18 and Bmi1 reveal synergy and requirement for maintenance but not initiation of Hox gene expression. *Development* **128**, 1587-1597.

Atsuta, T., Fujimura, S., Moriya, H., Vidal, M., Akasaka, T. and Koseki, H. (2001). Production of monoclonal antibodies against mammalian Ring1B proteins. *Hybridoma* **20**, 43-46.

Azcoitia, V., Aracil, M., Martinez-A, C. and Torres, M. (2005). The homeodomain protein Meis1 is essential for definitive hematopoiesis and vascular patterning in the mouse embryo. *Dev. Biol.* **280**, 307-320.

Blackledge, N. P., Farcas, A. M., Kondo, T., King, H. W., McGouran, J. F., Hanssen, L. L., Ito, S., Cooper, S., Kondo, K., Koseki, Y. et al. (2014). Variant PRC1 complex-dependent H2A ubiquitylation drives PRC2 recruitment and polycomb domain formation. *Cell* **157**, 1445-1459.

Boyer, L. A., Plath, K., Zeitlinger, J., Brambrink, T., Medeiros, L. A., Lee, T. I., Levine, S. S., Wernig, M., Tajonar, A., Ray, M. K. et al. (2006). Polycomb complexes repress developmental regulators in murine embryonic stem cells. *Nature* **441**, 349-353.

Cales, C., Roman-Trufero, M., Pavon, L., Serrano, I., Melgar, T., Endoh, M., Perez, C., Koseki, H. and Vidal, M. (2008). Inactivation of the polycomb group protein Ring1B unveils an antiproliferative role in hematopoietic cell expansion and cooperation with tumorigenesis associated with Ink4a deletion. *Mol. Cell. Biol.* **28**, 1018-1028.

Cao, R., Wang, L., Wang, H., Xia, L., Erdjument-Bromage, H., Tempst, P., Jones, R. S. and Zhang, Y. (2002). Role of histone H3 lysine 27 methylation in Polycomb-group silencing. *Science* **298**, 1039-1043.

Capdevila, J., Tsukui, T., Rodriquez Esteban, C., Zappavigna, V. and Izpisua Belmonte, J. C. (1999). Control of vertebrate limb outgrowth by the proximal factor Meis2 and distal antagonism of BMPs by Gremlin. *Mol. Cell* **4**, 839-849.

Cooper, K. L., Hu, J. K.-H., ten Berge, D., Fernandez-Teran, M., Ros, M. A. and Tabin, C. J. (2011). Initiation of proximal-distal patterning in the vertebrate limb by signals and growth. *Science* **332**, 1083-1086.

Cunningham, T. J., Chatzi, C., Sandell, L. L., Trainor, P. A. and Duester, G. (2011). Rdh10 mutants deficient in limb field retinoic acid signaling exhibit normal limb patterning but display interdigital webbing. *Dev. Dyn.* **240**, 1142-1150.

Cunningham, T. J., Zhao, X., Sandell, L. L., Evans, S. M., Trainor, P. A. and Duester, G. (2013). Antagonism between retinoic acid and fibroblast growth factor signaling during limb development. *Cell Rep.* **3**, 1503-1511.

del Mar Lorente, M., Marcos-Gutierrez, C., Perez, C., Schoorlemmer, J., Ramirez, A., Magin, T. and Vidal, M. (2000). Loss- and gain-of-function mutations show a polycomb group function for Ring1A in mice. *Development* **127**, 5093-5100.

Endoh, M., Endo, T. A., Endoh, T., Fujimura, Y.-I., Ohara, O., Toyoda, T., Otte, A. P., Okano, M., Brockdorff, N., Vidal, M. et al. (2008). Polycomb group proteins Ring1A/B are functionally linked to the core transcriptional regulatory circuitry to maintain ES cell identity. *Development* **135**, 1513-1524.

Endoh, M., Endo, T. A., Endoh, T., Isono, K.-I., Sharif, J., Ohara, O., Toyoda, T., Ito, T., Eskeland, R., Bickmore, W. A. et al. (2012). Histone H2A mono-ubiquitination is a crucial step to mediate PRC1-dependent repression of developmental genes to maintain ES cell identity. *PLoS Genet.* **8**, e1002774.

Gao, Z., Zhang, J., Bonasio, R., Strino, F., Sawai, A., Parisi, F., Kluger, Y. and Reinberg, D. (2012). PCGF homologs, CBX proteins, and RYBP define functionally distinct PRC1 family complexes. *Mol. Cell* **45**, 344-356.

Hisa, T., Spence, S. E., Rachel, R. A., Fujita, M., Nakamura, T., Ward, J. M., Devor-Henneman, D. E., Saiki, Y., Kutsuna, H., Tessarollo, L. et al. (2004). Hematopoietic, angiogenic and eye defects in Meis1 mutant animals. *EMBO J.* **23**, 450-459.

Isono, K., Endo, T. A., Ku, M., Yamada, D., Suzuki, R., Sharif, J., Ishikura, T., Toyoda, T., Bernstein, B. E. and Koseki, H. (2013). SAM domain polymerization links subnuclear clustering of PRC1 to gene silencing. *Dev. Cell* **26**, 565-577.

Kondo, T., Isono, K., Kondo, K., Endo, T. A., Itohara, S., Vidal, M. and Koseki, H. (2014). Polycomb potentiates meis2 activation in midbrain by mediating interaction of the promoter with a tissue-specific enhancer. *Dev. Cell* **28**, 94-101.

Kuzmichev, A., Nishioka, K., Erdjument-Bromage, H., Tempst, P. and Reinberg, D. (2002). Histone methyltransferase activity associated with a human multiprotein complex containing the Enhancer of Zeste protein. *Genes Dev.* **16**, 2893-2905.

Lanzuolo, C. and Orlando, V. (2012). Memories from the polycomb group proteins. *Annu. Rev. Genet.* **46**, 561-589.

Logan, M., Martin, J. F., Nagy, A., Lobe, C., Olson, E. N. and Tabin, C. J. (2002). Expression of Cre Recombinase in the developing mouse limb bud driven by a Prxl enhancer. *Genesis* **33**, 77-80.

Lynch, M. D., Smith, A. J. H., De Gobbi, M., Flenley, M., Hughes, J. R., Vernimmen, D., Ayyub, H., Sharpe, J. A., Sloane-Stanley, J. A., Sutherland, L. et al. (2012). An interspecies analysis reveals a key role for unmethylated CpG dinucleotides in vertebrate Polycomb complex recruitment. *EMBO J.* **31**, 317-329.

Mariani, F. V., Ahn, C. P. and Martin, G. R. (2008). Genetic evidence that FGFs have an instructive role in limb proximal-distal patterning. *Nature* **453**, 401-405.

Mercader, N., Leonardo, E., Azpiazu, N., Serrano, A., Morata, G., Martinez, C. and Torres, M. (1999). Conserved regulation of proximodistal limb axis development by Meis1/Hth. *Nature* **402**, 425-429.

Mercader, N., Leonardo, E., Piedra, M. E., Martinez, A. C., Ros, M. A. and Torres, M. (2000). Opposing RA and FGF signals control proximodistal vertebrate limb development through regulation of Meis genes. *Development* **127**, 3961-3970.

Mercader, N., Selleri, L., Criado, L. M., Pallares, P., Parras, C., Cleary, M. L. and Torres, M. (2009). Ectopic Meis1 expression in the mouse limb bud alters P-D patterning in a Pbx1-independent manner. *Int. J. Dev. Biol.* **53**, 1483-1494.

Niederreither, K., Vermot, J., Schuhbaur, B., Chambon, P. and Dolle, P. (2002). Embryonic retinoic acid synthesis is required for forelimb growth and anteroposterior patterning in the mouse. *Development* **129**, 3563-3574.

Oguro, H., Yuan, J., Ichikawa, H., Ikawa, T., Yamazaki, S., Kawamoto, H., Nakauchi, H. and Iwama, A. (2010). Poised lineage specification in multipotential hematopoietic stem and progenitor cells by the polycomb protein Bmi1. *Cell Stem Cell* **6**, 279-286.

Development (2016) 143, 276-285 doi:10.1242/dev.127506

Parr, B. A. and McMahon, A. P. (1995). Dorsalizing signal Wnt-7a required for normal polarity of D-V and A-P axes of mouse limb. *Nature* **374**, 350-353.

Pasini, D., Bracken, A. P., Hansen, J. B., Capillo, M. and Helin, K. (2007). The polycomb group protein Suz12 is required for embryonic stem cell differentiation. *Mol. Cell. Biol.* **27**, 3769-3779.

Probst, S., Kraemer, C., Demougin, P., Sheth, R., Martin, G. R., Shiratori, H., Hamada, H., Iber, D., Zeller, R. and Zuniga, A. (2011). SHH propagates distal limb bud development by enhancing CYP26B1-mediated retinoic acid clearance via AER-FGF signalling. *Development* **138**, 1913-1923.

Rosello-Diez, A., Ros, M. A. and Torres, M. (2011). Diffusible signals, not autonomous mechanisms, determine the main proximodistal limb subdivision. *Science* **332**, 1086-1088.

Schwarz, D., Varum, S., Zemke, M., Scholer, A., Baggiolini, A., Draganova, K., Koseki, H., Schubeler, D. and Sommer, L. (2014). Ezh2 is required for neural crest-derived cartilage and bone formation. *Development* **141**, 867-877.

Schwermann, J., Rathinam, C., Schubert, M., Schumacher, S., Noyan, F., Koseki, H., Kotlyarov, A., Klein, C. and Gaestel, M. (2009). MAPKAP kinase MK2 maintains self-renewal capacity of haematopoietic stem cells. *EMBO J.* **28**, 1392-1406.

Shi, X., Zhang, Z., Zhan, X., Cao, M., Satoh, T., Akira, S., Shpargel, K., Magnuson, T., Li, Q., Wang, R. et al. (2014). An epigenetic switch induced by Shh signalling regulates gene activation during development and medulloblastoma growth. *Nat. Commun.* **5**, 5425.

Simon, J. A. and Kingston, R. E. (2009). Mechanisms of polycomb gene silencing: knowns and unknowns. *Nat. Rev. Mol. Cell Biol.* **10**, 697-708.

Simon, J. A. and Kingston, R. E. (2013). Occupying chromatin: Polycomb mechanisms for getting to genomic targets, stopping transcriptional traffic, and staying put. *Mol. Cell* **49**, 808-824.

Tabin, C. and Wolpert, L. (2007). Rethinking the proximodistal axis of the vertebrate limb in the molecular era. *Genes Dev.* **21**, 1433-1442.

Tavares, L., Dimitrova, E., Oxley, D., Webster, J., Poot, R., Demmers, J., Bezstarosti, K., Taylor, S., Ura, H., Koide, H. et al. (2012). RYBP-PRC1 complexes mediate H2A ubiquitylation at polycomb target sites independently of PRC2 and H3K27me3. *Cell* **148**, 664-678.

Towers, M. and Tickle, C. (2009a). Generation of pattern and form in the developing limb. *Int. J. Dev. Biol.* **53**, 805-812.

Towers, M. and Tickle, C. (2009b). Growing models of vertebrate limb development. *Development* **136**, 179-190.

van Bakel, H., van Werven, F. J., Radonjic, M., Brok, M. O., van Leenen, D., Holstege, F. C. P. and Timmers, H. T. M. (2008). Improved genome-wide localization by ChIP-chip using double-round T7 RNA polymerase-based amplification. *Nucleic Acids Res.* **36**, e21.

van der Velden, Y. U., Wang, L., van Lohuizen, M. and Haramis, A.-P. G. (2012). The Polycomb group protein Ring1b is essential for pectoral fin development. *Development* **139**, 2210-2220.

van der Velden, Y. U., Wang, L., Querol Cano, L. and Haramis, A.-P. G. (2013). The Polycomb group protein ring1b/rnf2 is specifically required for craniofacial development. *PLoS ONE* **8**, e73997.

Voncken, J. W., Roelen, B. A. J., Roefs, M., de Vries, S., Verhoeven, E., Marino, S., Deschamps, J. and van Lohuizen, M. (2003). Rnf2 (Ring1b) deficiency causes gastrulation arrest and cell cycle inhibition. *Proc. Natl. Acad. Sci. USA* **100**, 2468-2473.

Wilkinson, D. G. and Nieto, M. A. (1993). Detection of messenger RNA by in situ hybridization to tissue sections and whole mounts. *Methods Enzymol.* **225**, 361-373.

Wu, H.-A., Balsbaugh, J. L., Chandler, H., Georgilis, A., Zullow, H., Shabanowitz, J., Hunt, D. F., Gil, J., Peters, G. and Bernstein, E. (2013). Mitogen-activated protein kinase signaling mediates phosphorylation of polycomb ortholog Cbx7. *J. Biol. Chem.* **288**, 36398-36408.

Wyngaarden, L. A., Delgado-Olguin, P., Su, I.-H., Bruneau, B. G. and Hopyan, S. (2011). Ezh2 regulates anteroposterior axis specification and proximodistal axis elongation in the developing limb. *Development* **138**, 3759-3767.

Yashiro, K., Zhao, X., Uehara, M., Yamashita, K., Nishijima, M., Nishino, J., Saijoh, Y., Sakai, Y. and Hamada, H. (2004). Regulation of retinoic acid distribution is required for proximodistal patterning and outgrowth of the developing mouse limb. *Dev. Cell* **6**, 411-422.

Yokobayashi, S., Liang, C.-Y., Kohler, H., Nestorov, P., Liu, Z., Vidal, M., van Lohuizen, M., Roloff, T. C. and Peters, A. H. F. M. (2013). PRC1 coordinates timing of sexual differentiation of female primordial germ cells. *Nature* **495**, 236-240.

Zeller, R., Lopez-Rios, J. and Zuniga, A. (2009). Vertebrate limb bud development: moving towards integrative analysis of organogenesis. *Nat. Rev. Genet.* **10**, 845-858.